JOURNAL OF NEUROTRAUMA 28:1767–1782 (September 2011)

DOI: 10.1089/neu.2010.1687

Quantitative Relationship between Axonal Injury and Mechanical Response in a Rodent Head Impact Acceleration Model

Yan Li, Liying Zhang, Srinivasu Kallakuri, Runzhou Zhou, and John M. Cavanaugh

Abstract

A modified Marmarou impact acceleration model was developed to study the mechanical responses induced by this model and their correlation to traumatic axonal injury (TAI). Traumatic brain injury (TBI) was induced in 31 anesthetized male Sprague-Dawley rats (392 ± 13 g) by a custom-made 450-g impactor from heights of 1.25 m or 2.25 m. An accelerometer and angular rate sensor measured the linear and angular responses of the head, while the impact event was captured by a high-speed video camera. TAI distribution along the rostro-caudal direction, as well as across the left and right hemispheres, was determined using β-amyloid precursor protein (β-APP) immunocytochemistry, and detailed TAI injury maps were constructed for the entire corpus callosum. Peak linear acceleration 1.25 m and 2.25 m impacts were 666 ± 165 g and 907 ± 501 g, respectively. Peak angular velocities were 95 ± 24 rad/sec and 124 ± 48 rad/sec, respectively. Compared to the 2.25-m group, the observed TAI counts in the 1.25-m impact group were significantly lower. Average linear acceleration, peak angular velocity, average angular acceleration, and surface righting time were also significantly different between the two groups. A positive correlation was observed between normalized total TAI counts and average linear acceleration ($R^2 = 0.612$, $p < 0.05$), and time to surface right ($R^2 = 0.545$, $p < 0.05$). Our study suggested that a 2.25-m drop in the Marmarou model may not always result in a severe injury, and TAI level is related to the linear and angular acceleration response of the rat head during impact, not necessarily the drop height.

Key words: corpus callosum; head impact acceleration model; linear and angular head motion; rat; traumatic axonal injury

Introduction

The rates of death and disability from severe head injuries remain very high despite a growing understanding of the pathomechanisms of traumatic brain injuries (TBI) and associated diffuse axonal injuries (DAI). DAI, more accurately described as traumatic axonal injury (TAI) (Smith and Meaney, 2000), is a well-recognized consequence of blunt head injury (Adams et al., 1982), and was originally described by Strich (1956) as diffuse degeneration of cerebral white matter (WM). Pathologically, TAI comprises diffuse and extensive lesions of the WM tracts (Blumbergs, 1997). TAI is produced by rapid head acceleration/deceleration during a traumatic event (Adams et al., 1982; Kelley et al., 2006), with consequent shear and tension on axons.

Much of the knowledge related to TAI comes from the extensive work of Povlishock (Povlishock and Becker, 1985; Povlishock, 1986,1992,1993), Gennarelli (Gennarelli et al., 1981,1998), and several other researchers (Marmarou and Povlishock 2006; Marmarou et al., 2006; Maxwell and Graham, 1997; Maxwell et al., 1988). In the period following a traumatic event, axonal damage is associated with large reactive swellings and retraction balls in various WM tracts throughout the brain. The pathogenesis of traumatically induced axonal damage is a complex process involving progressive lobulations that show accumulation of organelles and cytoskeletal components and their ultimate disconnection from the distal axonal segment (Povlishock et al., 1983; Yaghmai and Povlishock, 1992). Alterations in axonal cytoskeletal components have been attributed to impaired axoplasmic transport (IAT; Yaghmai and Povlishock, 1992), shown routinely by β-amyloid precursor protein (β-APP) immunocytochemistry (Stone et al., 2004). Other studies have shown that a traumatic event evokes focal alterations in axolemmal permeability, which was also shown to be associated with significant neurofilament compaction (NFC; Povlishock

Department of Biomedical Engineering, Wayne State University, Detroit, Michigan.

and Pettus, 1996). However, intra-axonal neurofilament compaction does not evoke local axonal swelling in all traumatically injured axons, and IAT and altered axolemmal permeability occur as distinct unrelated events (Stone et al., 2001). Widespread axonal degeneration associated with a traumatic event can lead to neuronal disconnection due to downstream synaptic degeneration and deafferentation of target postsynaptic cells (Rafols et al., 2007).

Knowledge of the relationship between the pathobiology and biomechanics of TBI has been gained by experimental evidence from various animal models, including the inertial rotational acceleration (Meaney et al., 1993; Ross et al., 1994), fluid percussion (Dixon et al., 1987; McIntosh et al. 1989; Povlishock et al., 1983), controlled cortical impact (Dixon et al., 1991; Lighthall, 1988), impact acceleration (Beaumont et al., 1999; Marmarou et al., 1994), and nerve stretch injury models (Dieterich et al., 2002; Gennarelli et al., 1989). Of these, the Marmarou impact acceleration (IA) model mimics a closed head injury induced by a combined linear and angular head impact, and is capable of producing significant TAI in discrete WM tracts, including the corpus callosum (CC) and brainstem in rats (Marmarou et al., 1994).

The Marmarou model has been used to characterize cellular and molecular responses to diffuse brain injury (Adelson et al., 2001; Kallakuri et al., 2007; Rafols et al., 2007; Thornton et al., 2006), as well as apoptosis and regeneration of neuronal cells following TBI (Cernak et al., 2002; Park and Yi, 2001; Tashlykov et al., 2007). The model has also been used to study attenuation of IAT and NFC following TBI (Marmarou et al., 2006; Stone et al., 2004). Motor and cognitive deficits induced by this model (Adelson et al., 1997,2000; Schmidt et al., 2000) have been studied, as well as oxidative stress and mitochondria-related injury (Tavazzi et al., 2005; Vagnozzi et al., 2007). Diagnoses and treatment after TBI using this model have also been extensively studied due to the graded TAI induced by different drop heights (Fei et al., 2006; Heath and Vink, 1999; Sengul et al., 2008).

In spite of the widespread utility of this model in studying various aspects of TBI there is a scarcity of work on the mechanical responses of the model (Gilchrist, 2004; Shafieian et al., 2009; Wang and Ma, 2010). Information on the relationship between measured rat head kinematics and the quantified axonal changes and other neuronal changes has not been investigated. Accordingly, the purposes of this study were (1) to characterize rat head kinematics following TBI of various severities in a modified version of the Marmarou IA model, (2) to quantify the extent of TAI throughout the CC in this model, and (3) to correlate the measured rat head kinematics to the quantified TAI changes in the CC.

Methods

Animal handling and preparation

Thirty-one anesthetized male Sprague-Dawley rats (392 ± 13 g) were used. TBI was induced by dropping a custom-made 450-g impactor housing a miniature accelerometer from a height of 1.25 m (n = 15) and 2.25 m (n = 16). The details of this modified model are the subject of a separate article. Briefly, this device uses a reinforced drop stand and an automatic release device to deliver consistent impact energy to rat head. The heights of 1.25 m and 2.25 m, although higher than those used in the original Marmarou model, were chosen to compensate for the loss of velocity caused by the accelerometer cable dragging against the tube (Zhang et al., 2010a). At these increased heights the actual impact velocities of 4.54 ± 0.06 m/sec and 6.14 ± 0.07 m/sec were close to the theoretical velocities of 4.43 m/sec and 6.26 m/sec, respectively, seen with drop heights of 1 m and 2 m.

All rats were administered buprenorphine (0.3 mg/kg) subcutaneously 20 min prior to impact. Fifteen minutes prior to impact, the rats were placed in a sealed acrylic chamber. Anesthesia was induced and maintained by a mixture of isofluorane (3%) and oxygen (0.6 L/min). The skull was exposed by a midline dorsal incision of the skin, and a round stainless steel disk (helmet) 10 mm in diameter and 3 mm thick was positioned at the midline between the bregma and the lambda and affixed to the skull vault using cyanoacrylate.

Impact acceleration device and instrumentation

The diffuse TBI device previously described by Marmarou and associates (1994) was modified for this study (Fig. 1A). In the original design, the diameter of the brass weight (impactor) was 18 mm. In the new design, the 450-g weight is made of an aluminum cylinder (length 126 mm, diameter 51 mm) to provide enough interior space to house an accelerometer, and a brass impact end (length 55 mm), tapered to 19 mm to create an impact interface similar to the original model. A miniature shock accelerometer was seated inside the 450-g impactor to measure the impact force on the helmet (Fig. 1B). The accelerometer cable passed through the top cover of the aluminum cylinder to connect to the data acquisition system (Fig. 1C). The 450-g weight was held at the desired height and released by a custom-made solenoid release device (Zhang et al., 2010a).

The linear response of the rat head was measured with a modified accelerometer. An angular rate sensor with its case removed and properly sealed was used to measure the angular velocity of the head in the sagittal plane. These two were glued together to the skull approximately 5 mm anterior to the helmet using cyanoacrylate (Fig. 1D). The use and application of these instruments has never been described for this model.

Signals from all of the transducers were acquired at a sampling rate of 10,000 Hz using the TDAS1R4 data acquisition system (Diversified Technical Systems, Inc., Seal Beach, CA). A high-speed video camera was used to record the impact event (Fig. 1E). Black and white targets were affixed to helmet and impactor for subsequent image tracking using the recorded video data. The video data was collected at 10,000 frames/sec during each experiment. The automatic weight release system, the transducer measuring system, and the camera system were synchronized through a trigger switch during the experiment.

Induction of traumatic brain injury

The instrumented animals were placed prone on an open-cell flexible polyurethane foam bed in pre-cured shape (12 × 12 × 43 cm; Foam to Size Inc., Ashland, VA) in an acrylic glass box under a 2.5-m-long 57-mm-diameter acrylic glass tube, with the helmet centered directly under the lower end of the tube. A laser beam was used to guide the positioning of the helmeted head to ensure that the impactor hit the center of the stainless steel disc (helmet) (Fig. 1E). Just prior to impact, the anesthesia was turned off. Then TBI was induced by dropping the weight from either 1.25 m or 2.25 m. Immediately after

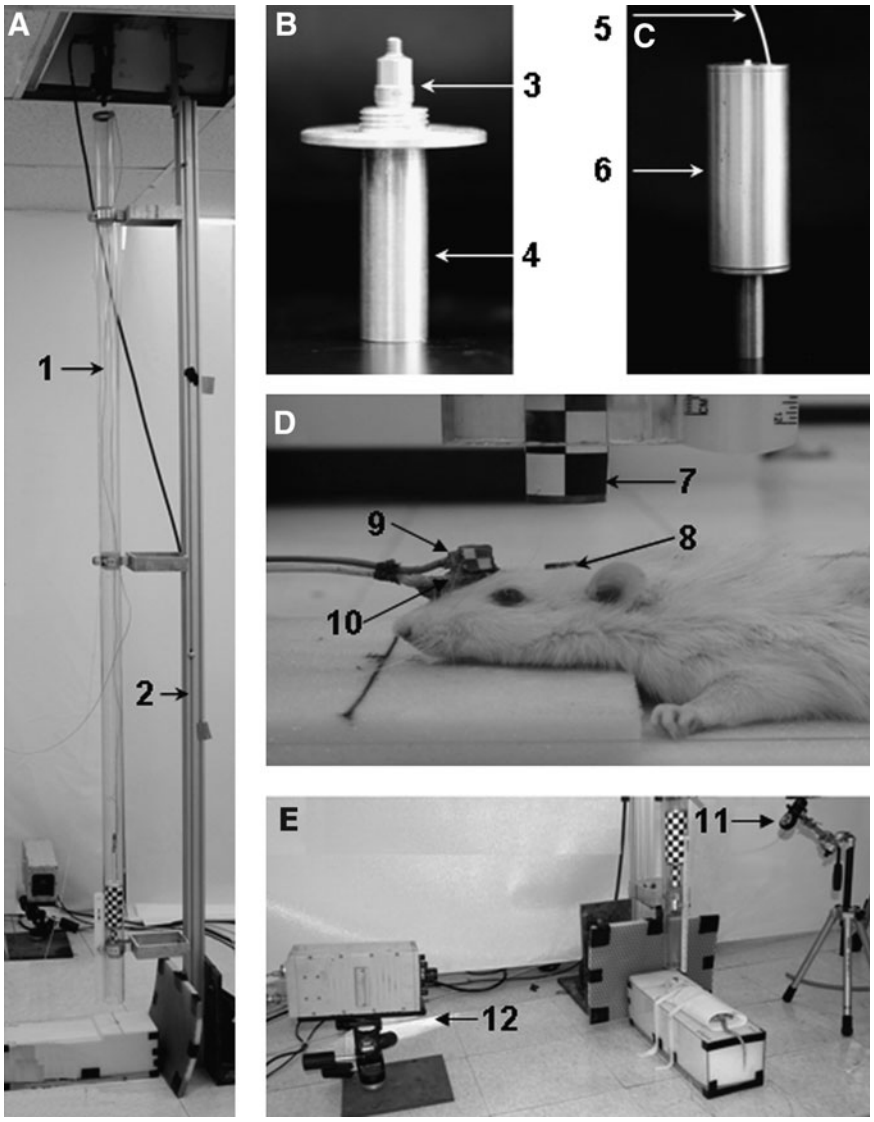

FIG. 1. Diagrams of the modified impact-acceleration injury model and instrumentation set-up (**A:** 1, acrylic glass tube; 2, aluminum pole; **B:** 3, accelerometer; 4, brass impact end; **C:** 5, accelerometer cable; 6, aluminum cylinder; **D:** 7, impactor; 8, helmet; 9, angular rate sensor; 10, accelerometer; 11, laser beam; **E:** 12, high-speed camera).

the impact, the acrylic glass box was manually removed to avoid a second impact to the rat head. After the removal of the stainless steel helmet and the transducers, the skull was examined for fractures and then the skin was closed with staples. Previous studies of the characterization of the foam mechanical properties suggested that viscoelastic softening could occur in the foam after the first compression, after that it reaches a steady state after the initial cycle, regardless of the number of subsequent cycles up to 3 weeks (Zhang et al., 2005,2011b). Therefore, a precompressed new piece of foam was used for a series of tests, and was subsequently replaced by a new one every 3 weeks to assure a consistent and repeatable mechanical response to a given impact.

Head impact data processing and analysis

The displacement of the impactor and the helmeted head were obtained digitally by tracking the attached target using image tracking software (ImageExpress MotionPlus; SAI, Utica, NY). Velocity change (dV) of the helmeted head was calculated by differentiating displacement-time histories of the head in the digitized video data. The velocity change of the rat head was also derived by integrating the linear head acceleration-time history. A reliable measurement of the rat head motion was ascertained when the head dV from the integrated acceleration signals reasonably matched to the head dV from video tracking, indicating that the sensors were rigidly attached to the skull during impact. Peak instantaneous linear acceleration a_{max} and average linear acceleration a_{avg} of the head were determined from the acceleration-time curve recorded by the accelerometer. a_{max} was the maximum absolute value of the negative portion of the head acceleration curve, and a_{avg} was the area under the negative portion of the curve divided by the time interval of that portion (Fig. 2A). Peak angular velocity ω_{max} and average angular velocity α_{avg} were determined from the angular velocity-time history

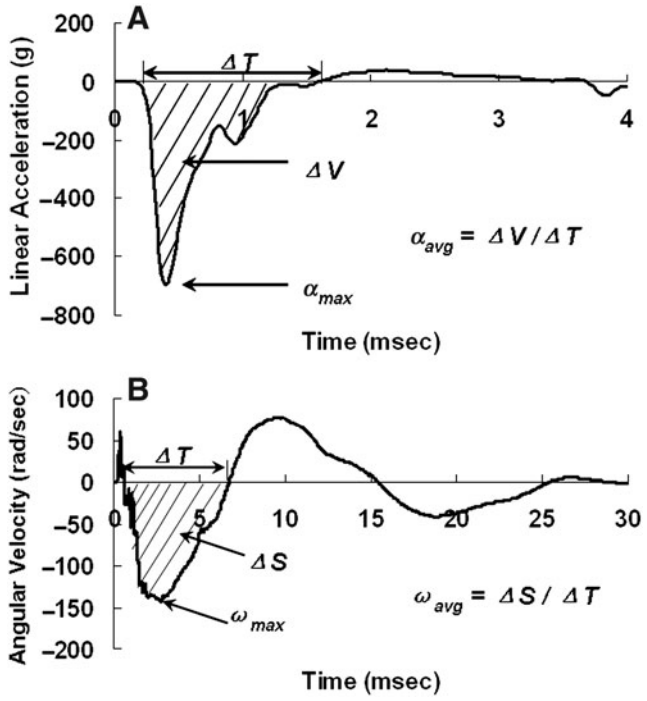

FIG. 2. Diagrams illustrating processing of data from the accelerometer and velocity sensors. (**A**) Method for obtaining peak and average linear acceleration from the linear acceleration time-history curve. (**B**) Method for obtaining peak and average angular velocity from the angular velocity-time history curve.

curves. ω_{max} was the maximum absolute value of the negative portion of the curve (initial counterclockwise rotation), and ω_{avg} was the area under the negative portion divided by the time interval of that portion (Fig. 2B). The angular velocity-time curve recorded from the angular rate sensor was filtered with a Society of Automotive Engineers channel class 1000 filter, and angular acceleration was obtained from the derivative of the angular velocity with respect to time. Peak α_{max} and average angular acceleration α_{avg} were then determined from the angular acceleration curve. α_{max} was the maximum absolute value of the negative portion of the curve, and α_{avg} was the area under the negative portion of the curve ($_{\Delta}\omega$) divided by the time interval ($_{\Delta}T$) of that portion.

Termination and fixation

After TBI, the rats were allowed to recover and monitored for at least 6 h. Rats with skull fractures or those exhibiting signs of severe distress were euthanized. After a 24-h survival period, each rat was euthanized with an overdose of sodium pentobarbital (120 mg/kg IP) and exsanguinated. The rats were then transcardially perfused with heparinized (500 units/mL) normal saline followed by cold 4% paraformaldehyde in phosphate-buffered saline (0.1 M PBS, pH 7.45). The brain was then carefully removed and post-fixed (4% paraformaldehyde in 30% sucrose), after which the cerebral hemispheres were coronally cut into 40-μm-thick frozen sections from the genu of the CC (+2.3 mm anterior to the bregma [0.00 mm]), through the splenium of the CC (−5.2 mm posterior to the bregma) based on the rat brain stereotaxic atlas (Paxinos and Watson, 2007). All the cut sections were individually placed in 1× PBS-filled multiwell plates and stored at 4°C until further processing. This enabled a subsequent precise selection of sections in close match with the coordinates indicated in the rat stereotaxic atlas.

Immunostaining for β-amyloid precursor protein-reactive axonal swellings and retraction balls

Thirteen to 15 coronal sections encompassing the anteroposterior aspects of the CC were selected and washed thoroughly in 1× PBS. The sections were spaced 0.48 mm apart. Of the 31 rats studied with 1.25-m and 2.25-m impacts, the majority (18 or 58%) had 14 sections, indicating consistency in section selection. Only a minority of rats had 13 (8 rats) and 15 sections (5 rats). The potential reason for the variability in the number of sections stained may be related to minor variations in the selection of the first section (starting after disappearance of the forceps minor and the beginning of the genu of the CC), and last section (at the end of the splenium and appearance of the forceps major). These sections were processed for antigen retrieval by incubation in a citrate buffer (pH 6.0) at 90°C for 1 h, and then washed 3 times in 1× PBS and allowed to cool to room temperature. They were subsequently immersed in 0.3% H_2O_2 for 1 h to quench endogenous peroxidase activity. This was followed by an overnight incubation (at room temperature) in C-terminus-specific β-APP antibody (1 μg/mL, rabbit anti-C-terminus β-APP, cat. no. #51-2700; Zymed, San Francisco, CA) in 2% normal goat serum (Vector Laboratories, Burlingame, CA) and 1% bovine serum albumin. The following day, the sections were washed 3 times for 5 min each in 1× PBS, and then incubated in goat anti-rabbit IgG secondary antibody (Vector Laboratories) for 1 h. The sections were visualized via incubation in avidin biotin peroxidase complex (Vectastain ABC Standard Elite Kit; Vector Laboratories), and were developed by brief incubation in 3,3′-diaminobenzidine (DAB) and hydrogen peroxide. Finally, the sections were washed, dehydrated, and cover-slipped using slide mounting medium. Control incubations were performed in the absence of primary antibody.

Quantitative analysis of traumatic axonal injury

The total number of β-APP-reactive axonal swellings and retraction balls (considered as total TAI counts) in the CC from all stained sections from each animal were quantified by a blinded observer. Each section was observed under a light microscope (Leica DMLB; Leica Microsystems Ltd., Heerburg, Switzerland) to visualize β-APP-reactive axonal swellings and retraction balls. Then serial photomicrographs (10× magnification) encompassing the whole CC were taken with a digital camera system (ProgRes C7; JENOPTIK Laser Optik Systeme, GmbH, Jena, Germany) of each section (13–15 sections/rat). These photomicrographs were taken at a single focal plane and were combined into a single panoramic image using Photoshop CS2. Then grids measuring 200×200 μm were superimposed on each constructed panoramic image. This enabled a direct correlation of the number of retraction balls and swellings with the level of mechanical strain in corresponding elements of the same resolution (~200×200 μm) in an anatomically detailed finite element

(FE) model of the rat head (Zhang et al., 2010a,2011b). All β-APP-reactive swellings and retraction balls in each grid were counted using ImageJ software (http://rsb.info.nih.gov/ij/), and added to obtain total TAI counts per section. The total TAI in the CC for each rat was the sum of TAI from panoramic images of all stained sections. In order to compare TAI levels between rats with different section numbers, TAI counts were normalized based on Eq. 1; 14 was used as a normalizing constant in the equation, since the majority of rats (18 out of 31) had 14 sections.

$$\text{Normalized TAI} = (\text{total TAI}/\text{number of sections}) \times 14 \quad [1]$$

Finite element analysis of impact angle effect on traumatic axonal injury distribution

Finite element simulations of the Marmarou impact acceleration model could provide insight into the mechanical response phenomena that may not be adequately explained by the transducer measurements or pathophysiological observations for TAI resulting from this complex system. An anatomically inspired, detailed FE model of the adult Sprague-Dawley rat head, which consisted of the scalp, skull, dura, arachnoid-pia, gray and white matter of the cerebrum and cerebellum, ventricles, corpus callosum, brainstem with pyramidal tract and medial lemniscus, cervical spine, and facial tissues, along with the rest of body (over 960,000 elements) was developed and validated (Zhang et al., 2010b). This rat model was integrated with a validated FE foam model (Zhang et al., 2011b) to simulate the rat head impact acceleration tests (Zhang et al., 2010b,2011a). In the current study, the resulting maximum principal strain distribution in the CC was assessed to explain the distribution of the TAI counts in relation to the location of the impact. Additionally, the model was set up to simulate and quantify the influences of helmet surface angles on the resulting three-dimensional head acceleration and the localized tissue strain distribution across the rat brain hemispheres during impact (Fig. 3). More specifically, the helmet was inclined at 5° to the left in the coronal plane with respect to the bottom surface of the impactor.

Statistical analysis

Given values were mean ± standard deviation (SD). A paired *t*-test was used to assess the statistical significance of each mechanical response and the TAI count between the two drop heights. A p value < 0.05 was considered to be statistically significant. Linear regression and analysis of variance (ANOVA) were used to evaluate the correlation between mechanical responses and TAI.

Results

Biomechanical parameters

The average impact velocities for the 1.25-m and 2.25-m experimental groups were 4.54 ± 0.06 m/sec and 6.14 ± 0.07 m/sec, respectively. During 1.25-m impacts (Fig. 4), the rat head excursion was 72.2 ± 3.4 mm into the foam within a span of 28.6 ± 0.8 msec. During 2.25-m impacts, the amount of head excursion increased to 90.4 ± 4.9 mm within 28.9 ± 0.5 msec (Fig. 4). The consistency in depth and duration of foam compression at each impact height indicated the reliability of the energy transfer induced by this modified model.

During impacts from both heights, the rat head experienced very high linear and angular accelerations in the initial 2–4 msec (Fig. 5). Peak linear acceleration was 666 ± 165 g and 907 ± 501 g for impacts from 1.25 m and 2.25 m, respectively, and was reached within 1 msec. Peak angular velocity in the sagittal plane was 95 ± 24 rad/sec and 124 ± 48 rad/sec for 1.25-m and 2.25-m impacts, respectively, and was reached within 3 msec. As revealed by the acceleration data, the rat head experienced both linear and angular motions during the impact. The overall mechanical responses from 1.25-m and 2.25-m impacts are summarized in Table 1. Among the biomechanical responses measured and calculated, average linear acceleration, peak angular velocity, and average angular acceleration were significantly different between the 1.25-m and 2.25-m groups ($p < 0.05$; Fig. 6A, B, and C).

Physiological variables and mortality

There were no skull fractures or mortalities following TBI from 1.25 m height. However, there was a 10.2% mortality rate, and 20.4% rats showed skull fractures following TBI from 2.25 m. Only two rats out of 16 studied in the 2.25-m drop group showed signs of severe respiratory depression necessitating artificial respiratory support in the form of chest massage to encourage spontaneous breathing with intermittent delivery of 0.6 L oxygen (0.6 L/min) via a nose cone. In rats impacted from 1.25 m no obvious respiratory depression was observed. The duration of recovery from impact in the

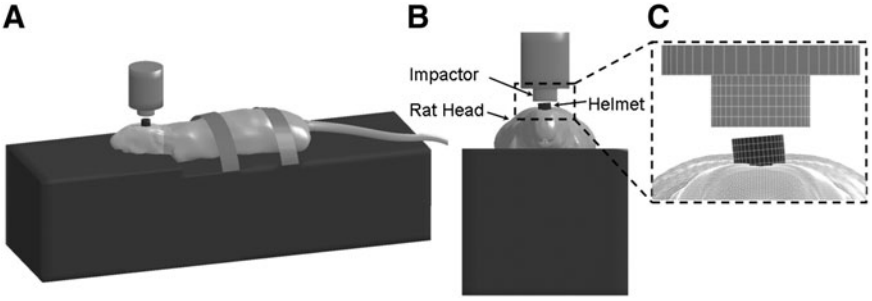

FIG. 3. Lateral (**A**), anterior (**B**), and close up (**C**) views of the computer model simulation set-up for Marmarou's rat head impact acceleration experiments, with the helmet surface inclined at 5° to the left or right in the coronal plane with respect to the bottom surface of the impactor.

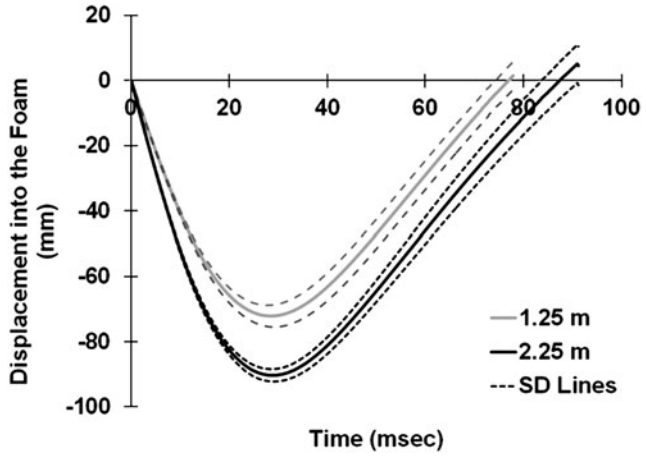

FIG. 4. Graph of displacement of the rat head into the foam. Since the impactor remained in close contact with the rat head during the impact, markers on the impactor were tracked to reflect the displacement of the rat head into the foam during the impact. The displacement curves (solid line) represent the average value from 1.25-m and 2.25-m drop tests. The dashed lines represent the standard deviation range.

form of surface righting latency was also measured for all rats. The latency to surface righting reflex was 31.4 ± 20.1 min in 2.25-m group, which was significantly longer than the average of 18.9 ± 12.2 min observed in the 1.25-m group ($p < 0.05$; Fig. 6D). In rats impacted from 2.25 m, moderate epidural hemorrhage confined to the dorsal aspect of the cerebral hemispheres was observed. Modest blood pooling at the base of the skull extending up to C3–C4 spinal cord was also observed in some of these animals. No other focal injuries were observed. These changes were not observed in animals impacted from 1.25 m.

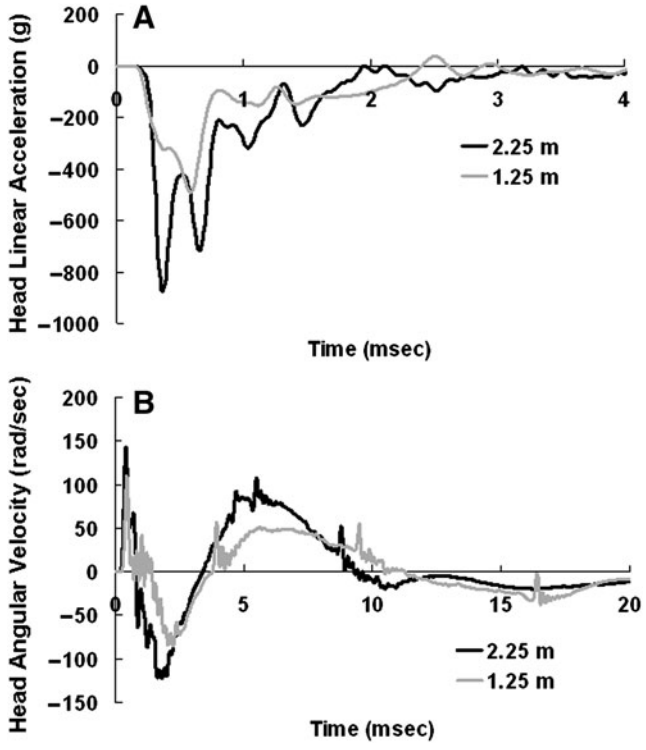

FIG. 5. (**A**) Representative time history curves of rat head linear acceleration recorded by the accelerometer for impacts from 1.25 m and 2.25 m. (**B**) Representative time history curves of rat head angular velocity from the angular rate sensor for impacts from 1.25 m and 2.25 m.

Traumatic axonal injury assessment and quantification

To our knowledge, this is the first study using the Marmarou IA model to perform a detailed quantification of TAI in a series of sections encompassing the entire CC. β-APP immunocytochemistry revealed axonopathy in the form of reactive axonal swellings and retraction balls across the entire CC. In each panoramic section of the CC, the TAI injury count was determined in each 200×200-μm grid (Fig. 7). The higher intensity prominently occurred in rats impacted from 2.25 m, and to a lesser degree in rats impacted from 1.25 m (see section on TAI quantification). In the current report, the CC was the only structure where axonal changes were quantified through the entire structure. TAI was also observed in the pyramidal tracts (Fig. 8A), the pyramidal decussation (Fig. 8B), the junction of the CC and the alveus (Fig. 8C), the ventral hippocampal commissure (Fig. 8D), the fibers of the median eminence (Fig. 8E), and the cingulum (Fig. 8F). Other areas observed with TAI include the external capsule, and areas of the septal nucleus, fimbria, dorsal hippocampus optic chiasm, and preoptic area. The complete quantification of TAI severity and extent in the major tracts of the brainstem is part of a separate investigation.

A set of 13–15 sections were quantified and from each section an injury map was constructed (Fig. 9). Over 370 injury maps of the CC were constructed for 31 rats. The normalized total TAI counts per rat in the CC were 186 ± 230 for the 2.25-m group and 20 ± 13 for the 1.25-m group. The normalized total TAI count was significantly higher in the 2.25-m group compared to the 1.25-m group ($p < 0.05$; Fig. 6E).

The spatial profiles of the TAI maps revealed a nonuniform distribution longitudinally along the CC (Fig. 10B), with the area directly under the helmet, in particular from 0.12–2.04 mm posterior to the bregma, showing higher densities of TAI. This portion of CC under the helmet may have experienced higher skull deformation and compression and potentially experienced higher combined linear and angular acceleration, compared to the caudal part of the CC under the helmet, since the rat head first rotated counterclockwise during impact. The FE simulation of the head impact also showed a concentrated region of high strain in the same CC region below the helmet (Fig. 10C). The direct force transformation through the skull may induce higher strain in the cortex and CC under the impact site compared to more peripheral regions. This trend was a consistent finding in axonal injury maps in the entire CC structure.

Fourteen out of 16 rats analyzed expressed a fairly symmetrical distribution of TAI on both sides of the midline (Fig. 11). This result agreed with the fact that head motion was mainly in the sagittal plane during impact. However, we identified asymmetric accumulations of β-APP in two rats, suggesting potential lateralization of the impact, leading to uneven distribution of the impact energy. This condition may be caused by a slight angle between the impactor surface and the angled helmet surface.

Table 1. Mechanical Responses of the Rat Head to 1.25-m and 2.25-m Weight Drop

	Biomechanical responses, mean ± standard deviation						
Test	*Impact velocity (m/sec)*	*Peak linear acceleration (g)*	*Average linear acceleration (g)*	*Peak angular velocity (rad/sec)*	*Average angular velocity (rad/sec)*	*Peak angular acceleration (krad/sec^2)*	*Average angular acceleration (krad/sec^2)*
2.25 m ($n = 16$)	6.14 ± 0.07	907 ± 501	293 ± 156	124 ± 48	63 ± 24	178 ± 59	73 ± 33
1.25 m ($n = 15$)	4.54 ± 0.06	666 ± 165	154 ± 46	95 ± 24	47 ± 17	169 ± 37	51 ± 32

Correlation between mechanical response and traumatic axonal injury

Although initial impact velocity and energy transfer were consistent during impact, there were variations between rats in the acceleration responses and the total TAI count for both groups, but more so in the 2.25-m group. A quantitative analysis between total TAI counts and average head acceleration revealed a positive linear relationship, with the regression equation being $Y = 1.018X - 124.46$ ($R^2 = 0.612$, $p < 0.05$; Fig. 12A). Of the 16 cases in the lower portion of the graph bounded by average accelerations of 100–200 g and TAI counts of 0–50, 13 were from the 1.25-m drop height. We have also observed that of the 16 cases for the 2.25-m drop height, 7 had relatively low values of average linear acceleration (less than 200 g). There was also significant linear correlation between the total TAI count and the time to surface right ($R^2 = 0.545$, $p < 0.05$; Fig. 12B). These results indicate that higher average head accelerations produced more injury in the CC, and led to longer times to surface right (prolonged time to regain consciousness).

Discussion

Model improvement

The Marmarou IA model is one of the most widely used preclinical models to study diffuse brain injury in rats. As discussed, results from this study offer for the first time the

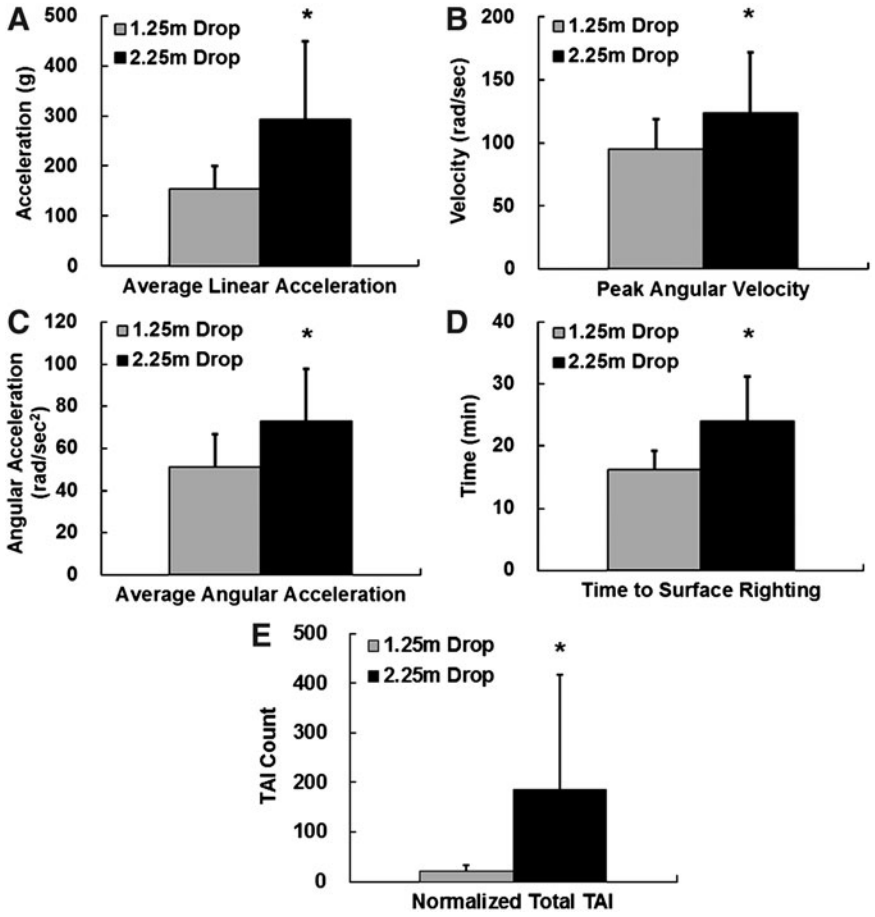

FIG. 6. Bar graphs show comparisons of biomechanical responses, surface righting, and traumatic axonal injury (TAI) counts for the 1.25-m and 2.25-m drop tests. (**A**) Average linear acceleration. (**B**) Peak angular velocity. (**C**) Average angular acceleration. (**D**) Time to perform surface righting. (**E**) Normalized total TAI counts.

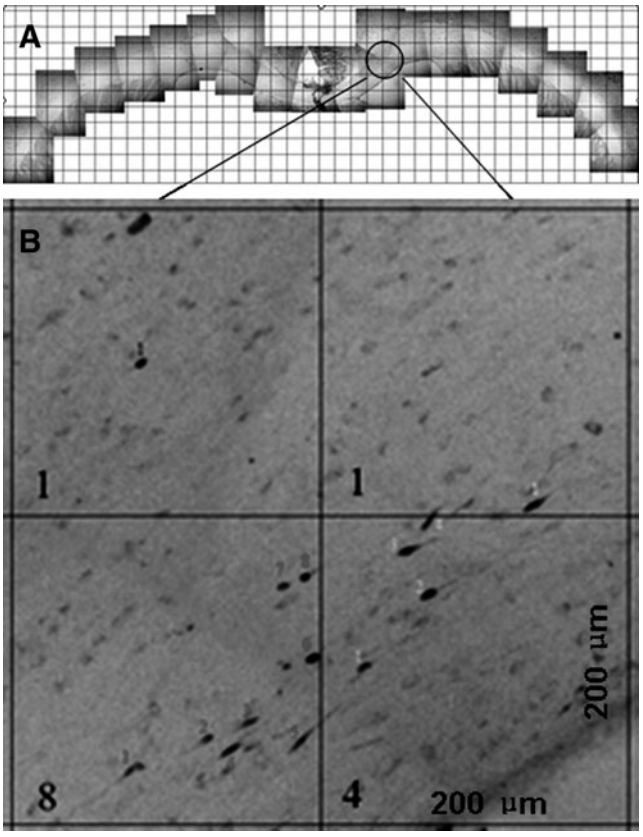

FIG. 7. Quantification of traumatic axonal injury (TAI) in the corpus callosum. (**A**) A representative panoramic view of the corpus callosum used to quantify β-amyloid precursor protein (β-APP)-reactive (+) axonal profiles. (**B**) An example of quantification of TAI in 200×200-μm boxes. The number at the left lower corner indicates the TAI count in each box.

comparison of various mechanical parameters with TAI. As part of the current study, the model has been modified and expanded to monitor velocity, displacement into the foam, head linear acceleration, and head angular velocity, during impact injury of various severities.

In an earlier kinematic study of the Marmarou IA device, Piper and colleagues (1996) measured velocity by placing a photo-conductance cell near the bottom of the acrylic glass tube, and they found that the velocity of the 450-g weight dropped from a height of 2 m can vary by as much as 40% depending on the degree of initial friction. They indicated that the use of supporting fishing line through the eye of a metal wing nut resulted in less variation in weight drop velocity, with fewer episodes of line breakage or depressed skull fracture. Others reported that friction between the metal weight and vertical tube changed over time (Carré et al., 2004; Ucar et al., 2006), which can also lead to variations in velocity. However, results from our modified model showed that head impact velocities from both 2.25-m (6.14 ± 0.07 m/sec) and 1.25-m (4.54 ± 0.06 m/sec) heights were consistent within the same drop height. This modified device utilizes a rigid support frame for the drop tower and reduced impactor length, as well as an automatic release mechanism, which may reduce variations in impact velocity. Other system errors such as stiffness of the foam bed (Piper et al., 1996) and lateral movement of the weight inside the acrylic glass tube (Cernak, 2005) were closely monitored in our modified system. Fatigue of the foam bed can be indentified by the displacement curve (Fig. 4), if an outlier occurs. Accumulation of β-APP on one side of the cerebral hemisphere on the injury map (Fig. 11) usually indicates an angled lateral impact, as discussed later. We also provided a 50-min interval between impacts and changed the foam after about 20 impacts (Zhang et al., 2011b). The potential variations in the mechanical systems described may also be major contributors to the varying mortality rates reported by different groups: 56.8% by Pascual and colleagues (2007) (no ventilator support), 41% by Geeraerts and colleagues (2006) (with ventilator support), 35.7% by Rhodes and colleagues (2002) (with ventilator support), 31% by Ueda and colleagues (2001) (no ventilator support), 20% by Fei and colleagues (2007) (with ventilator support), 15% by Suehiro and colleagues (2001) (with ventilator support), and 10% by Marmarou and colleagues (2006) (with ventilator support). The mortality rate in the current study was 10% for 2.25-m impacts, which is similar to that of the original model using ventilator support (Marmarou et al., 2006). Taken together,

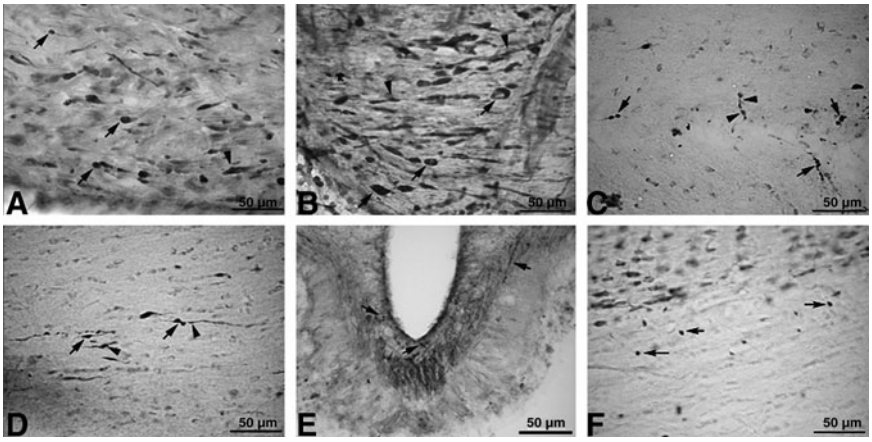

FIG. 8. Photomicrographs showing traumatic axonal injury (TAI) evidenced by β-amyloid precursor protein (β-APP)-reactive retraction balls (arrows), or swollen regions (arrowheads) appearing as a string of beads (arrowhead in **C**), were seen in the pyramidal tracts (**A**), the pyramidal decussation (**B**), the junction of the corpus callosum and the alveus (**C**), the ventral hippocampal commissure (**D**), the median eminence (**E**), and the cingulum (**F**).

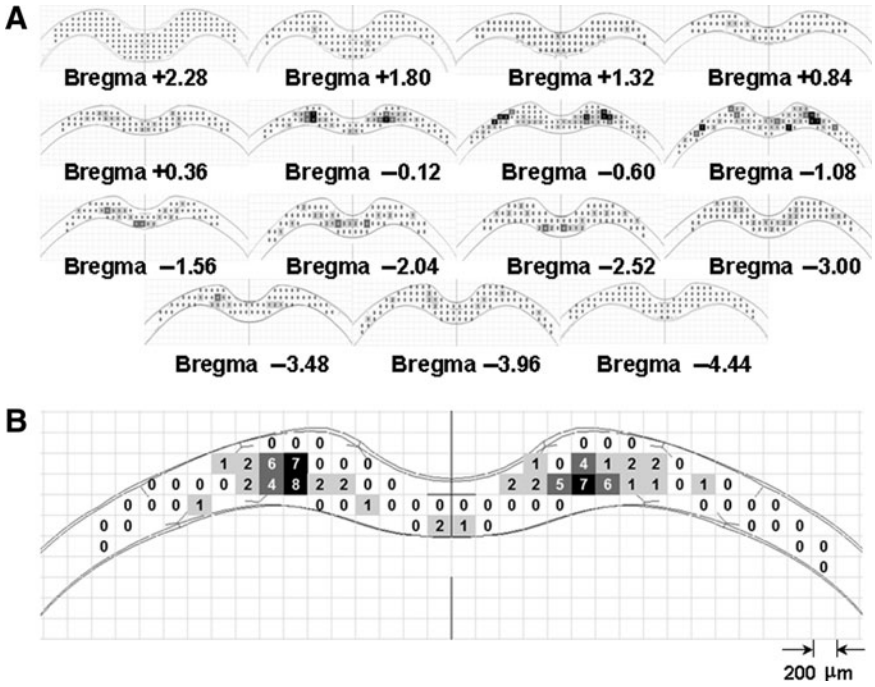

FIG. 9. Injury maps. (**A**) A set of injury maps from one representative rat impacted from the 2.25-m drop height at different corpus callosum (CC) locations relative to the bregma. (**B**) A representative injury map showing the distribution of traumatic axonal injury (TAI) in the CC. Different colors were assigned for varying TAI counts (light grey = 0–3 TAI counts; dark grey = 4–6 TAI counts; black > 6 TAI counts).

the modifications reported in the current device may help standardize the use of this model.

A limitation of this model is the large variation we observed in impact biomechanics (Table 1) and total TAI counts in the 2.25-m impacts. Seven out of 16 rats in the 2.25-m impact group only showed minimal TAI as shown by β-APP immunoreactivity. These results suggest that the 2.25-m drop in this modified Marmarou's model may not always result in a severe injury. Our hypothesis is that the TAI level is related to linear/angular acceleration during impact, and not necessarily the drop height. One factor that may cause the variability of the system is the helmet surface angle at initial impact. A computer model simulation was conducted to identify the influences of helmet surface angles on the resulting head acceleration in the lateral direction, which may contribute to the asymmetrical pattern of the axonal counts. As the helmet was tilted about 5° from horizontal in the coronal plane (Fig. 3), the condition resulted in 56%, 17%, and 10% increases, in x, z, and resultant accelerations, respectively, with an additional y acceleration of 400 g compared to the helmet surface aligned at a perfectly horizontal level. Similarly in head rotational acceleration, the angled impact resulted in a decrease of rotational acceleration in the sagittal plane, and induced an additional rotation in the coronal plane. As a result, the brain strain difference between the left and right hemispheres was about 10%. If the extent of axonal pathology was mediated by white matter strain, the asymmetric axonal profile would be associated with the initial impactor/helmet contact condition. Future tests will include a tri-axial angular rate sensor to capture the head kinematics in all axes.

The lack of precise control over impact conditions can result in a high degree of variability in this model, making the injury response difficult to reproduce between different investigators and laboratories. In order to standardize the use of this model, especially when certain aspects of TBI severity need to be quantified, we recommend paying close attention to weight drop velocity, tube stability, foam condition, impactor-helmet interface, and length of return to consciousness in the animal. Specific recommendations are as follows. (1) Initially measure the weight drop velocity in each system. The impact velocity can be obtained either by a velocity trap device (Piper et al., 1996), or high-speed video analysis as in the current study. (2) Use a support frame for the acrylic tube that is stable such as the one used in the current study. (3) Use measures to insure consistent foam stiffness. According to our previous study, 30% stress softening could occur during the second test compared to the response of new foam (Zhang et al., 2011b). The stress behavior of a used foam for the subsequent tests remains the same as for the second cycle for up to 3 weeks. If another test needs to be conducted in less than 1 h, a piece of used foam or a piece of new foam that has been compressed to about 90 mm 1 h prior to the actual test could assure the repeatability of the resilience of the foam material in the tests. The use of new foam for each test is another alternative to attain repeatable results, but the stress-strain characteristics between the new and used foam are different (Zhang et al., 2011b). If the equipment is available it is recommended that the elastic properties of the foam bed be determined and tracked periodically (Piper et al., 1996). (4) Since lateral movement of the impactor and helmet surface angles may potentially cause uneven distribution of the impact energy to the helmet/head, and thus increase variability of outcomes, a laser beam was used in our study to

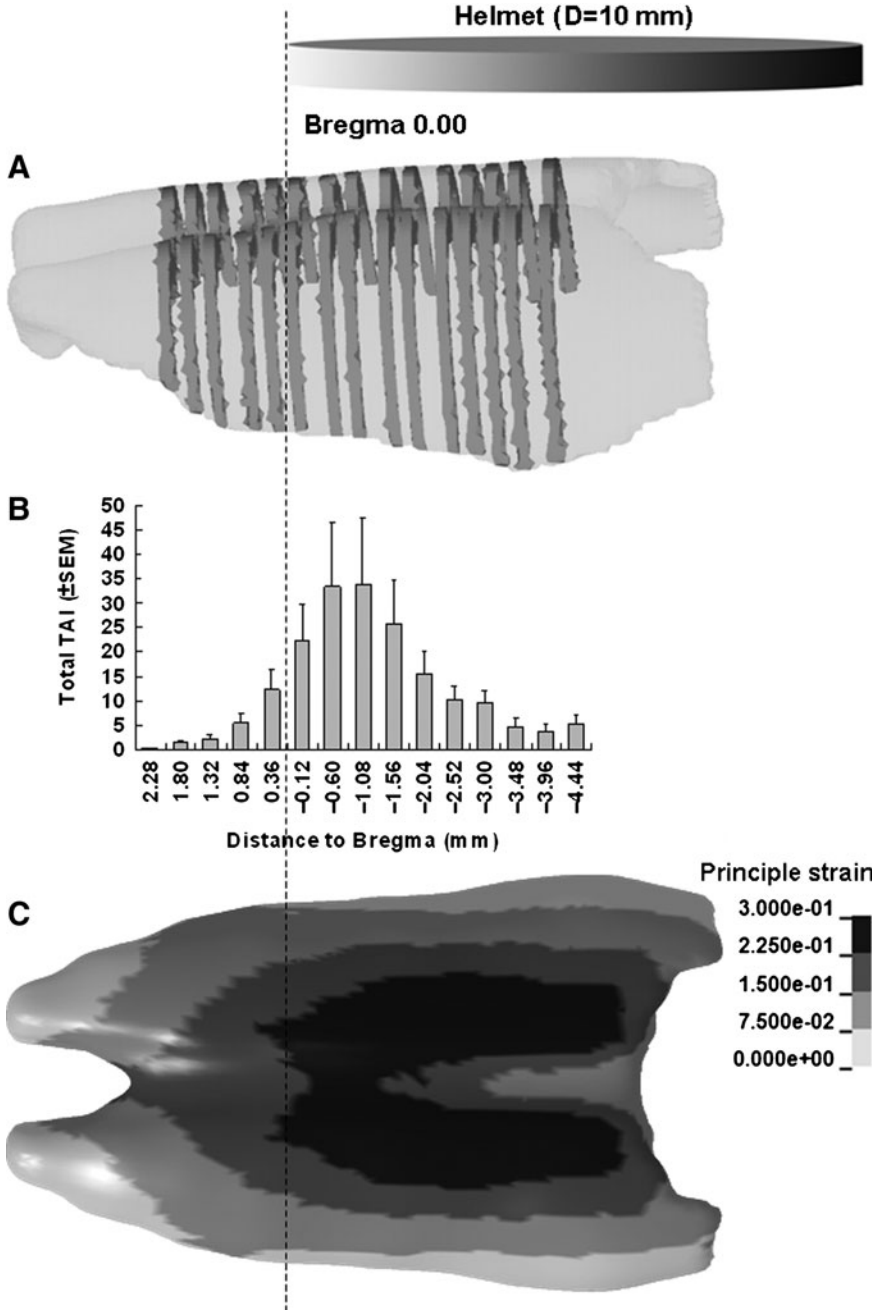

FIG. 10. Traumatic axonal injury (TAI) distribution along the rostro-caudal direction in 2.25-m impacted rats. The relative position of the 10-mm-diameter helmet is also shown. (**A**) Illustration of sections selected from the genu of the corpus callosum (CC) through the splenium of the CC. (**B**) Bar graph showing average TAI numbers in sections at the given anatomical locations along the rostro-caudal direction. (**C**) A case showing strain distribution predicted in the CC of the rat head finite element model for the 2.25-m drop height (SEM, standard error of the mean).

guide the positioning of the rat head under the acrylic glass tube, and high-speed video was used to check the alignment of the impactor and helmet at initial impact. With or without such equipment, careful alignment of the weight by centering it directly above the helmet is important prior to the impact. (5) Post-injury behavior, such as duration of loss of consciousness and time to surface right, can aid in assessing injury severity and help to exclude outliers. Where the equipment is available, monitoring the dynamic response of the rat head will provide measures that correlate to injury severity, and enable comparison of TAI levels between different research groups.

Biomechanical parameters

To our knowledge, the present study is the first to characterize *in vivo* mechanical responses of the rat head subjected to TBI by the Marmarou IA model. Both linear and angular motions of the rat head were directly recorded and analyzed. In the original Marmarou model, a mathematical

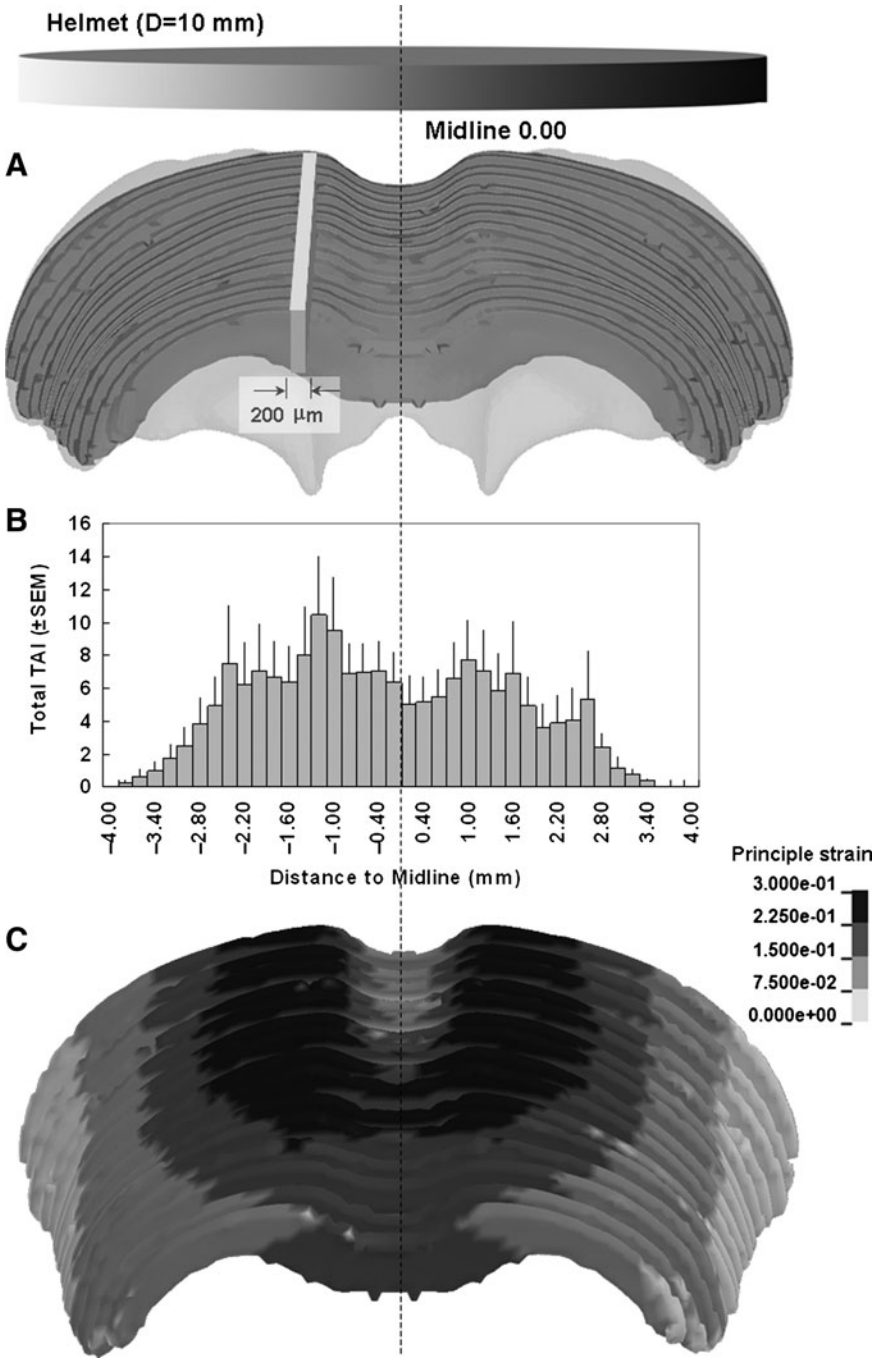

FIG. 11. Traumatic axonal injury (TAI) distribution across the left and right hemispheres in 2.25-m-impacted rats. (**A**) Demonstration of a cuboid (width = 0.2 mm, height = height of the corpus callosum [CC], length = distance from the genu of the CC to the splenium of the CC), selected at the sagittal plane of the CC for TAI counting. (**B**) Bar graph showing the average TAI numbers in the corresponding 0.2-mm-thick cuboids shown in (**A**) at given anatomical locations across the left and right hemispheres. (**C**) A case showing strain distribution predicted in the CC of the rat head finite element model for 2.25-m drop height (SEM, standard error of the mean).

analysis was used to calculate the peak linear acceleration of the rat head (Marmarou et al., 1994). In their model stimulation, acceleration was very brief, lasting approximately 0.2 msec from peak to zero, with peak magnitudes of 900 g for 2-m and 630 g for 1-m impacts. Results from our current study showed similar average peak linear accelerations of 907 g and 666 g for 2.25-m and 1.25-m drops, respectively, albeit with a longer duration of approximately 2 msec. The longer duration in acceleration from the current study may be related to differences in material properties in the rat head compared to the spring-damper properties assumed in the mathematical model. The passive correlation of the average head acceleration to TAI counts also suggested that both the magnitude and duration of head acceleration contributed

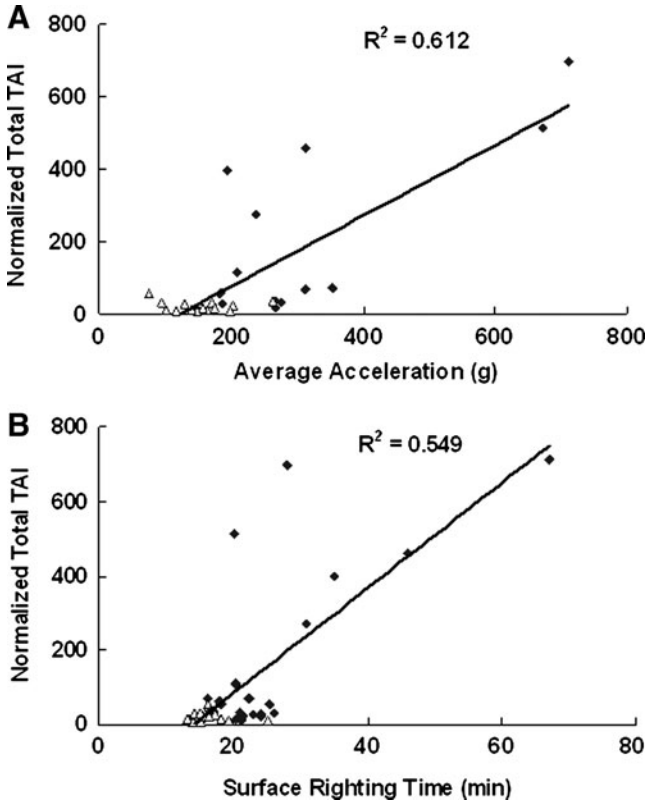

FIG. 12. The relationship between normalized total traumatic axonal injury (TAI) counts and average linear acceleration (**A**), and surface righting time (**B**). Rhombus symbols represent data from 2.25-m drop, and triangle symbols represent data from 1.25-m drop.

to the occurrence of axonal damage and the associated extent of injury.

The peak angular acceleration values of 178 krad/sec^2 (at 2.25 m) and 169 krad/sec^2 (at 1.25 m) in our study were lower than the values reported by Fijalkowski and colleagues (2007) in their pure coronal plane angular acceleration model relevant to concussive injury. In their study, rats subjected to peak angular accelerations of 368 ± 30 krad/sec^2 showed perineuronal vacuolation as evidenced by hematoxylin and eosin staining, with minimal axonal injury in the CC as indicated by β-APP staining. Another rat model combining linear and angular accelerations (Wang et al., 2010) showed that angular acceleration of 137 ± 12 krad/sec^2 resulted in no evidence of TAI in the CC by β-APP staining, but a combination of linear and angular acceleration could produce TAI consistently. Taken together, these studies indicate that TAI in current rat models is potentially induced by linear acceleration or a combination of linear and angular acceleration. This notion is further supported by previous biomechanical studies (Duma et al., 2005; King et al., 2003; Viano et al., 2005; Walilko et al., 2005), suggesting that high non-impact angular acceleration alone may not be sufficient to produce TAI, but a combination of linear and angular accelerations may play a pivotal role in the production of TAI.

Several previous studies examined the relationship between axonal injury and mechanical loading in species other than the rat. Gennarelli and associates (1982) published one of the earliest studies on the relationship between the mechanical response of the tissue and axonal injury in primates subjected to acceleration injury. They found that the amount of TAI strongly correlated with the direction of the head angular motion, with motions about the coronal plane producing the highest TAI magnitude and duration of coma. Further studies suggested that increased TAI severity was related to rotational kinematics, including angular velocity (Meaney et al., 1995), angular acceleration (Margulies and Thibault, 1992), and duration of acceleration (Gennarelli et al., 1982), using non-impact rotational acceleration models. Anderson and colleagues (2003), using a sheep blunt impact acceleration model, suggested that the most reliable predictors for the extent of axonal injury were peak linear velocity and peak angular velocity.

However, studies aimed at correlating biomechanical responses with injury level in rat IA models are limited. Most previous studies assessed TAI level based on drop height (Czeiter et al., 2008; Sawauchi et al., 2004; Vagnozzi et al., 2005), but did not quantify the mechanical response of the head. Results from our current study showed that in spite of minimal variations in impactor velocity, biomechanical responses in the rat head can vary widely within the same drop height. This may be related to small variations between the angle of the impactor surface and the helmet surface, variations in head shape and size, an eccentric line of action of the contact force, and thickness of the skull. On the other hand, assessing which characteristics of an impact (e.g., force, energy, and acceleration) best predict the risk of TAI is of particular importance in developing injury criteria used by regulatory agencies that provide standards for the design and manufacture of safety equipment and motor vehicles. Accordingly, we attempted to directly correlate rat kinematics with TAI level, and found that average head acceleration showed promise as an injury predictor. Lissner and associates (1960) showed similar results in human cadaver testing. The Wayne State Tolerance Curve (WSTC) demonstrated that the severity of head injury was dependent both on the magnitude and duration of average or effective impact acceleration. The average head acceleration is also the basis of the existing Head Injury Criteria (HIC) used by most regulatory agencies when assessing the safety of motor vehicles (Prasad and Mertz, 1985). In a future study we will seek to identify the injury threshold based on additional measured biomechanical parameters.

Traumatic axonal injury quantification

TAI marked by β-APP immunoreactivity was observed in various WM tracts of rats impacted from both 2.25 m and 1.25 m, indicating the utility of this modified model in inducing widespread axonal pathology. The presence of TAI in the CC, internal capsule, optic tracts, cerebral and cerebellar peduncles, and the long tracts in the brainstem was consistent with previous studies that showed axonal pathology in similar locations in the original Marmarou model (Czeiter et al., 2008; Kallakuri et al., 2003; Marmarou et al., 1994; Rafols et al., 2007; Stone et al., 2001). Our results also showed that the extent of TAI was significantly greater at 2.25 m than at 1.25 m, which agrees with a preliminary study by Kallakuri and associates (2003), showing that TAI in the CC was most severe in the 2-m group, and mildest in the 1-m group.

A more detailed quantification of TAI in the CC was undertaken in this study than in previous studies using the Marmarou AI device. One silver impregnation study reported profiles of TAI as swellings, retraction balls, and axons with vacuoles, in four sections through the CC for each rat, using three rats at each drop height (Kallakuri et al., 2003). Another study (DiLeonardi et al., 2009) identified TAI in 2D panoramic images of the CC from three anatomic locations, and described temporal and spatial progression of TAI at these locations, but TAI counts were not reported. Furthermore, by utilizing 13–15 sections across the entire CC, the spatial profiles of TAI maps revealed non-uniform distribution longitudinally along the CC, with the area directly under the helmet (bregma 0.60/0.84 mm) showing a higher density of TAI in some rats.

Smith and Meaney (2000) showed that the pattern of axonal damage in the WM is more accurately described as multifocal. Therefore, TAI from a limited number of selected locations may not be an accurate representation of injury profiles in the entire CC. Utilizing the quantified data from many sections in our study, 3D injury maps were constructed and graded for the entire CC. In each panoramic section of CC, the TAI injury count was determined in each 200×200-μm grid. These sections were used to create injury maps to permit an element-by-element correlation with the mechanical response (such as the brain strain along with the rate at which the strain is applied) predicted at that location by the FE rat head model as shown in Fig. 10C and Fig. 11C.

The current study utilized β-APP immunoreactivity, which is a marker for IAT. However, TAI involves both IAT as well as NFC labeled by RMO14 (Marmarou et al., 2005; Stone et al., 2001). Hence, immunostaining with RMO14 antibody, quantification of NFC, generation of injury maps for NFC, and merging these maps with those generated by β-APP immunoreactivity is the focus of ongoing work. The combined results are necessary to provide a thorough depiction of the extent of TAI produced by various pathomechanisms, and their relationship to the underlying mechanical response in TBI.

Ongoing studies quantifying TAI in pyramidal tracts will provide further information on the degree of the involvement of the brainstem that occurs in TBI. The correlation of severity and distribution of axonal damage in varying sites of the brain with the mechanical responses of impact may offer further insights into understanding the mechanistic mechanisms of TBI in WM tracts.

Translation to human injury models

FE models provide a promising technique to study the mechanical response of the human brain to blunt trauma and the stresses and strains in brain tissue that lead to brain injury. Cadaver tests have been used to validate the mechanical response of FE models (King et al., 1995; Zhang et al., 2001a,2001b,2001c,2004). However, cadavers lack viable neural tissue, and although precise mechanical input can be measured, TAI cannot be assessed. The TAI injury maps developed in the current rat study will be correlated to tissue level stresses and strains in a rat head FE model (Zhang et al., 2010a,2011b). This will allow determination of tissue thresholds for TAI. The goal is to translate such tissue thresholds to human head models, and thereby enhance the capability of the human head model to predict brain injury.

Conclusions

In the current study, a modified impact acceleration model was developed to characterize the rat head kinematics for various TAI severities. Both linear and angular motion of the rat head during dynamic impact were recorded and analyzed. The density and distribution of TAI through the CC was also quantified, and 3D injury maps were constructed for each experimental rat. The results showed a positive correlation between TAI in the CC and average head acceleration and time to surface right. Our study suggests that TAI level is related to linear and angular accelerations of the rat head during impact and not necessarily the drop height. The model shows promise in elucidating the relationship between the extent of cellular injury and the mechanical response, which is not possible with biomechanical cadaveric studies or in animal TBI studies, in which the mechanical response is not measured.

Acknowledgments

The work was supported by National Institutes of Health grant R01 EB006508.

Author Disclosure Statement

No competing financial interests exist.

References

Adams, J.H., Graham, D.I., Murray, L.S., and Scott, G. (1982). Diffuse axonal injury due to nonmissile head injury in humans: an analysis of 45 cases. Ann. Neurol. 12, 557–563.

Adelson, P.D., Dixon, C.E., and Kochanek, P.M. (2000). Long-term dysfunction following diffuse traumatic brain injury in the immature rat. J. Neurotrauma 17, 273–282.

Adelson, P.D., Dixon, C.E., Robichaud, P., and Kochanek, P.M. (1997). Motor and cognitive functional deficits following diffuse traumatic brain injury in the immature rat. J. Neurotrauma 14, 99–108.

Adelson, P.D., Jenkins, L.D., and Hamilton, R.L. (2001). Histopathologic response of the immature rat to diffuse traumatic brain injury. J. Neurotrauma 18, 967–976.

Anderson, R.W.G., Brown, C.J., Blumbergs, P.C., McLean, A.J., and Jones, N.R. (2003). Impact mechanics and axonal injury in a sheep model. J. Neurotrauma 20, 961–974.

Beaumont, A., Marmarou, A., Czigner, A., Yamamoto, M., Demetriadou, K., and Shirotani, T. (1999). The impact-acceleration model of head injury: injury severity predicts motor and cognitive performance after trauma. Neurol. Res. 21, 742–754.

Blumbergs, P.C. (1997). Pathology, in: *Head Injury*. P. Reilly, and R. Bullock (eds). Chapman & Hill: London, pps. 39–70.

Carré, E., Cantais, E., Darbin, O., Terrier, J.P., Lonjon, M., Palmier, B., and Risso, J.J. (2004). Technical aspects of an impact acceleration traumatic brain injury rat model with potential suitability for both microdialysis and PtiO2 monitoring. J. Neurosci. Methods 30, 23–28.

Cernak, I. (2005). Animal models of head trauma. NeuroRx 2, 410–422.

Cernak, I., Chapman, S.M., Harnlin, G.P., and Vink, P. (2002). Temporal characterization of pro- and anti-apoptotic mechanisms following diffuse traumatic brain injury in rats. J. Clin. Neurosci. 9, 565–572.

Czeiter, E., Pal, J., Kovesdi, E., Bukovics, P., Luckl, J., Doczi, T., and Buki, A. (2008). Traumatic axonal injury in the spinal

cord evoked by traumatic brain injury. J. Neurotrauma 25, 205–213.

Dieterich, D.C., Bockers T.M., and Gundelfinger, E.D. (2002). Screening for differentially expressed genes in the rat inner retina and optic nerve after optic nerve crush. Neurosci. Lett. 317, 29–32.

DiLeonardi, A.M., Huh, J.W., and Raghupathi, R. (2009). Impaired axonal transport and neurofilament compaction occur in separate populations of injured axons following diffuse brain injury in the immature rat. Brain Res. 1263, 174–182.

Dixon, C.E., Clifton, G.L., Lighthall, J.W., Yaghmai, A.A., and Hayes, R.L. (1991). A controlled cortical impact model of traumatic brain injury in the rat. J. Neurosci. Methods 39, 253–262.

Dixon, C.E., Lyeth, B.G., Povlishock, J.T., Findling, R.L., Hamm, R.J., and Marmarou, A. (1987). A fluid percussion model of experimental brain injury in the rat. J. Neurosurg. 67, 110–119.

Duma, S.M., Manoogian, S.J., Bussone, W.R., Brolinson, P.G., Goforth, M.W., Donnenwerth, J.J., Greenwald, R.M., Chu, J.J., and Crisco, J.J. (2005). Analysis of real-time head accelerations in collegiate football players. Clin. J. Sport Med. 15, 3–8.

Fei, Z., Zhang, X., and Bai, H.M. (2006). Metabotropic glutamate receptor antagonists and agonists: potential neuroprotectors in diffuse brain injury. J. Clin. Neurosci. 13, 1023–1027.

Fei, Z., Zhang, X., Bai, H.M., Jiang, X.F., Li, X., Zhang, W., and Hu, W. (2007). Posttraumatic secondary brain insults exacerbates neuronal injury by altering metabotropic glutamate receptors. BMC Neurosci. 17, 96.

Fijalkowski, R.J., Stemper, B.D., Pintar, F.A., Yoganandan, N., Crowe, M.J., and Gennarelli T.A. (2007). New rat model for diffuse brain injury using coronal plane angular acceleration. J. Neurotrauma 24, 1387–1398.

Foda, M.A., and Marmarou, A. (1994). A new model of diffuse brain injury in rats, Part II: morphological characterization. J. Neurosurg. 80, 301–313.

Geeraerts, T., Ract, C., Tardieu, M., Fourcade, O., Mazoit, J.X., Benhamou, D., Duranteau, J., and Vigué, B. (2006). Changes in cerebral energy metabolites induced by impact-acceleration brain trauma and hypoxic-hypotensive injury in rats. J. Neurotrauma 23, 1059–1071.

Gennarelli, T.A., Adams, J.H., and Graham, D.I. (1981). Acceleration induced head injury in the monkey. I. The model, its mechanical and physiological correlates. Acta Neuropathol. Suppl. (Berl.) 7, 23–25.

Gennarelli, T.A., Thibault, L.E., Adams, J.H., Graham, D.I., Thompson, C.J., and Marcincin, R.P. (1982). Diffuse axonal injury and traumatic coma in the primate. Ann. Neurol. 12, 564–574.

Gennarelli, T.A., Thibault, L.E., and Graham, D.I. (1998). Diffuse axonal injury: An important form of traumatic brain damage. Neuroscientist 4, 202–215.

Gennarelli, T.A., Thibault, L.E., and Tipperman, R. (1989). Axonal injury in the optic nerve: a model simulating diffuse axonal injury in the brain. J. Neurosurg. 71, 244–253.

Gilchrist, M.D. (2004). Experimental device for simulating traumatic brain injury resulting from linear accelerations. Strain 40, 180–192.

Heath, D.L., and Vink, R. (1999). Improved motor outcome in response to magnesium therapy received up to 24 hours after traumatic diffuse axonal brain injury in rats. J. Neurosurg. 90, 504–509.

Kallakuri, S., Kreipke, C.W., Rossi, N., Rafols, J.A., and Petrov, T. (2007). Spatial alterations in endothelin receptor expression are temporally associated with the altered microcirculation after brain trauma. Neurol. Res. 29, 362–368.

Kelley, B.J., Farkas, O., Lifshitz, J., and Povlishock, J.T. (2006). Traumatic axonal injury in the perisomatic domain triggers ultrarapid secondary axotomy and Wallerian degeneration. Exp. Neurol. 198, 350–360.

King, A.I., Ruan, J.S., Zhou, C., Hardy, W.N., and Khalil, T.B. (1995). Recent advances in biomechanics of brain injury research. J. Neurotrauma 12, 651–658.

King, A.I., Yang, K.H., Zhang, L., and Hardy, W. (2003). Is head injury caused by linear or angular acceleration? Proceedings of IRCOBI Conference, Lisbon, Portugal, pps. 1–12.

Lighthall, J.W. (1988). Controlled cortical impact: a new experimental brain injury model. J. Neurotrauma 5, 1–15.

Lissner, H.R., Lebow, M., and Evans, G. (1960). Experimental studies on the relation between acceleration and intracranial pressure changes in man. Surg. Gynec. Obst. U.S.A. 111, 329–338.

Margulies, S.S., and Thibault, L.E. (1992). A proposed tolerance criterion for diffuse axonal injury in man. J. Biomech. 25, 917–923.

Marmarou, A., Foda, M.A., Brink, W.V., Campbell, J., Kita, H., and Demetriadou, K. (1994). A new model of diffuse brain injury in rats. Part I: Pathophysiology and biomechanics. J. Neurosurg. 80, 291–300.

Marmarou, A., Signoretti, S., Aygok, G., Fatouros, P., and Portella, G. (2006). Traumatic brain edema in diffuse and focal injury: cellular or vasogenic? Acta Neurochir. Suppl. 96, 24–29.

Marmarou, C.R., and Povlishock, J.T. (2006). Administration of the immunophilin ligand FK506 differentially attenuates neurofilament compaction and impaired axonal transport in injured axons following diffuse traumatic brain injury. Exp. Neurol. 197, 353–362.

Marmarou, C.R., Walker, S.A., Davis, C.L., and Povlishock, J.T. (2005). Quantitative analysis of the relationship between intra-axonal neurofilament compaction and impaired axonal transport following diffuse traumatic brain injury. J. Neurotrauma 22, 1066–1080.

Maxwell, W.L., and Graham, D.I. (1997). Loss of axonal microtubules and neurofilaments after stretch-injury to guinea pig optic nerve fibers. J. Neurotrauma 14, 603–614.

Maxwell, W.L., Kansagra, A.M., Graham, D.I., Adams, J.H., and Gennarelli, T.A. (1988). Freeze-fracture studies of reactive myelinated nerve fibres after diffuse axonal injury. Acta Neuropathol. (Berl.) 76, 395–406.

McIntosh, A.D., Kallieris, D., Mattern, R., and Miltner, E. (1989). Traumatic brain injury in the rat: Characterization of a lateral fluid-percussion model. Neuroscience 28, 233–244.

Meaney, D.F., Smith, D.H., Ross, D.T., and Gennarelli, T.A. (1993). Diffuse axonal injury in miniature pig: Biomechanical development and injury threshold. Cashworthiness and Occupant Protection in Transportation Systems, ASME, 169, 169–175.

Meaney, D.F., Smith, D.H., Shreiber, D.I., Brain, A.C., Miller, R.T., Ross, D.T., and Gennarelli, T.A. (1995). Biomechanical analysis of experimental diffuse axonal injury. J. Neurotrauma 12, 689–694.

Park, C.O., and Yi, H.G. (2001). Apoptotic change and NOS activity in the experimental animal diffuse axonal injury model. Yosei Med. J. 42, 518–526.

Pascual, J.M., Solivera, J., Prieto, R., Barrios, L., López-Larrubia, P., Cerdán, S., and Roda, J.M. (2007). Time course of early metabolic changes following diffuse traumatic brain injury in

rats as detected by (1)H NMR spectroscopy. J. Neurotrauma 24, 944–959.

Paxinos, G., and Watson, C. (2007). *The Rat Brain in Stereotaxic Coordinates*, 6th ed. Academic Press: Sydney.

Piper, I.R., Thomson, D., and Miller, J.D. (1996). Monitoring weight drop velocity and foam stiffness as an aid to quality control of a rodent model of impact acceleration neurotrauma. J. Neurosci. Methods 69, 171–174.

Povlishock, J.T. (1993). Pathobiology of traumatically induced axonal injury in animals and man. Ann. Emerg. Med. 22, 980–986.

Povlishock, J.T., and Becker, D.P. (1985). Fate of reactive axonal swellings induced by head injury. Lab. Invest. 52, 540–552.

Povlishock, J.T., Becker, D.P., Cheng, C.L., and Vaughan, G.W. (1983). Axonal change in minor head injury. J. Neuropathol. Exp. Neurol. 42, 225–242.

Povlishock, J.T. (1992). Traumatically induced axonal injury: pathogenesis and pathobiological implications. Brain Pathol. 2, 1–12.

Povlishock, J.T. (1986). Traumatically induced axonal damage without concomitant change in focally related neuronal somata and dendrites. Acta Neuropathol. (Berl.) 70, 53–59.

Povlishock, J.T., and Pettus, E.H. (1996). Traumatically induced axonal damage: evidence for enduring changes in axolemmal permeability with associated cytoskeletal change. Acta Neurochir. Suppl. 66, 81–86.

Prasad, P., and Mertz, H.J. (1985). The position of the United States Delegation to the ISO working group 6 on the use of HIC in the automotive environment. SAE, Paper No. 851246.

Rafols, J.A., Morgan, R., Kallakuri, S., and Kreipke, C.W. (2007). Extent of nerve cell injury in Marmarou's model compared to other brain trauma models. Neurol. Res. 29, 348–355.

Rhodes, J.K., Andrews, P.J., Holmes, M.C., and Seckl, J.R. (2002). Expression of interleukin-6 messenger RNA in a rat model of diffuse axonal injury. Neurosci. Lett. 335, 1–4.

Ross, D.T., Meaney, D.F., Sabol, M.K., Smith, D.H., and Gennarelli, T.A. (1994). Distribution of forebrain diffuse axonal injury following inertial closed head injury in miniature swine. Exp. Neurol. 126, 291–299.

Sawauchi, S., Marmarou, A., Beaumont, A., Signoretti, S., and Fukui, S. (2004). Acute subdural hematoma associated with diffuse brain injury and hypoxemia in the rat: effect of surgical evacuation of the hematoma. J. Neurotrauma 21, 563–573.

Sengul, G., Takci, E., Malcok, U.A., Akar, A., Erdogan, F., Kadioglu, H.H., and Aydin, I.H. (2008). A preliminary histopathological study of the effect of agmatine on diffuse brain injury in rats. J. Clin. Neurosci. 15, 1125–1129.

Schmidt, R.H., Scholten, K.J., and Maughan, P.H. (2000). Cognitive impairment and synaptosomal choline uptake in rats following impact acceleration injury. J. Neurotrauma 17, 1129–1139.

Shafieian, M., Darvish, K.K., and Stone, J.R. (2009). Changes to the viscoelastic properties of brain tissue after traumatic axonal injury. J. Biomech. 42, 2136–2142.

Smith, D.H., and Meaney, D.F. (2000). Axonal damage in traumatic brain injury. Neuroscientist 6, 483–494.

Stone, J.R., Okonkwo, D.O., Dialo, A.O., Rubin, D.G., Mutlu, L.K., Povlishock, J.T., and Helm G.A. (2004). Impaired axonal transport and altered axolemmal permeability occur in distinct populations of damaged axons following traumatic brain injury. Exp. Neurol. 190, 59–69.

Stone, J.R., Singleton, R.H., and Povlishock, J.T. (2001). Intraaxonal neurofilament compaction does not evoke local axonal swelling in all traumatically injured axons. Exp. Neurol. 172, 320–331.

Strich, S.J. (1956). Diffuse degeneration of the cerebral white matter in severe dementia following head injury. J. Neurol. Neurosurg. Psychiatry 19, 163–185.

Suehiro, E., Singleton, R.H., Stone, J.R., and Povlishock, J.T. (2001). The immunophilin ligand FK506 attenuates the axonal damage associated with rapid rewarming following posttraumatic hypothermia. Exp. Neurol. 172, 199–210.

Tashlykov, V., Katz, Y., Gazit, V., Zahar, O., Schreiber, S., and Pick, C.G. (2007). Apoptotic changes in the cortex and hippocampus following minimal brain trauma in mice. Brain Res. 1130, 197–205.

Tavazzi, B., Signoretti, S., Lazzarino, G., Amorini, A.M., Delfini R., Cimatti, M., Marmarou, A., and Vagnozzi, R. (2005). Cerebral oxidative stress and depression of energy metabolism correlate with severity of diffuse brain injury in rats. Neurosurgery 56, 582–589.

Thornton, E., Vink, R., and Blumbergs, P.C. (2006). Soluble amyloid precursor protein alpha reduces neuronal injury and improves functional outcome following diffuse traumatic brain injury rats. Brain Res. 1094, 38–46.

Ucar, T., Tanriover, G., Gurer, I., Onal, M.Z., and Kazan, S. (2006). Modified experimental mild traumatic brain injury model. J. Trauma 60, 558–565.

Ueda, T., Iwata, A., Komatsu, H., Aihara, N., Yamada, K., Ugawa, S., and Shimada, S. (2001). Diffuse brain injury induces local expression of Na+/myo-inositol cotransporter in the rat brain. Brain Res. Mol. Brain Res. 86, 63–69.

Vagnozzi, R., Signoretti, S., Tavazzi, B., Cimatti, M., Amorini, A.M., Donzelli, S., Delfini, R., and Lazzarino, G. (2005). Hypothesis of the postconcussive vulnerable brain: experimental evidence of its metabolic occurrence. Neurosurgery 57, 164–171.

Vagnozzi, R., Tavazzi, B., Signoretti, S., Amorini, A.M., Belli, A., Cimatti, M., Delfini, R., DiPietro, V., Finocchiaro, A., and Lazzarino, G. (2007). Temporal window of metabolic brain vulnerability to concussions: mitochondrial-related impairment-part I. Neurosurgery 61, 379–388.

Viano, D.C., Casson, I.R., Pellman, E.J., Zhang, L., Yang, K.H., and King, A.I. (2005). Concussion in professional football: Brain responses by finite element analysis—Part 9. Neurosurgery 57, 891–916.

Walilko, T.J., Viano, D.C., and Bir, C.A. (2005). Biomechanics of the head for Olympic boxer punches to the face. Br. J. Sports Med. 39, 710–719.

Wang, H.C., Duan, Z.X., Wu, F.F., Xie, L., Zhang, H., and Ma, Y.B. (2010). A new rat model for diffuse axonal injury using a combination of linear acceleration and angular acceleration. J. Neurotrauma 27, 707–719.

Wang, H.C., and Ma, Y.B. (2010). Experimental models of traumatic axonal injury. J. Clin. Neurosci. 17, 157–162.

Yaghmai, A., and Povlishock, J.T. (1992). Traumatically induced reactive change as visualized through the use of monoclonal antibodies targeted to neurofilament subunits. J. Neuropathol. Exp. Neurol. 51, 158–176.

Zhang, L., and Yang, K.H. (2001a). Biomechanics of neurotrauma. Neurol. Res. 23, 144–156.

Zhang, L., Gurao, M., Yang, K.H., and King, A.I. (2011b). Material characterization and computer model simulation of low density polyurethane foam used in a rodent traumatic brain injury model. J. Neurosci. Methods 198, 93–98.

Zhang, L., Gurao, M., Yang, K.H., and King, A.I. (2005). Material characterization of low density polyurethane foam used for

traumatic brain injury modeling, in: Proceedings of ASME Bioengineering Conference No. 54807, American Society of Mechanical Engineers.

Zhang, L., Li, Y., and Cavanaugh, J.M. (2010a). A new measuring system to quantify head kinematics in a rodent model of traumatic axonal injury, in: Proceedings of IBIA 8th World Congress on Brain Injury 2010, International Brain Injury Association.

Zhang, L., Yang, K.H., and King, A.I. (2004). A proposed injury threshold for mild traumatic brain injury. J. Biomech. Eng. 126, 226–236.

Zhang, L., Yang, K.H., and King, A.I. (2001b). Comparison of brain responses between frontal and lateral impacts by finite element modeling, J. Neurotrauma 18, 21–30.

Zhang, L., Yang, K.H., Dwarampudi, R., Omori, K., Li, T., Chang, K., Hardy, W.N., Khalil, T.B., and King, A.I. (2001c). Recent advances in brain injury research: A new human head model development and validation. Stapp Car Crash J. 45, 369–393.

Zhang, L., Zhou, R., and Cavanaugh, J.M. (2011a). Quantitative correlation of brain strain with traumatic axonal injury using a combined computer and experimental model of rat head impact acceleration induced TBI. J. Neurotrauma 28, A-26.

Zhang, L., Zhou, R., and Yue, N. (2010b). Biomechanical response of impact acceleration-induced traumatic axonal injury: rat head model development and injury localization. J. Neurotrauma 26, A-18.

Address correspondence to:
Liying Zhang, Ph.D.
Department of Biomedical Engineering
Wayne State University
818 W. Hancock Street
Detroit, MI 48201

E-mail: lzhang@wayne.edu